

A solution to generalized learning from small training sets found in infants’ repeated visual experiences of individual objects

Frangil M. Ramirez¹
fraramir@iu.edu

Elizabeth Clerkin²
emclerki@iu.edu

David J. Crandall¹
djcran@iu.edu

Linda B. Smith²
smith4@iu.edu

¹Department of Computer Science, Luddy School of Informatics, Computing, and Engineering

²Department of Psychological and Brain Sciences

^{1,2}Indiana University, Bloomington, IN 47405

Abstract

One-year-old infants show immediate adult-like generalization of common object categories to novel instances. The field has limited understanding of how this early prowess is achieved. Here we provide evidence on infants’ daily-life visual experiences for 8 early-learned object categories. Using a corpus of infant head camera images recorded at mealtimes (87 mealtimes captured by 14 infants), we quantify the individual instances experienced by infants and the similarity structure of all images containing an instance of each category. The distribution of instances is highly skewed, containing, for each infant and category, many images of the same few objects along with fewer images of other instances. Graph theoretic measures of the similarity structure for individual categories reveal a “lumpy” mix of high similarity and high variability, organized into multiple but interconnected clusters of high-similarity images. In computational experiments, we show that creating training sets that include an oversampling of varied images from a single instance yields a “lumpy” similarity structure. We also show that these artificially-created training sets support generalization to novel instances after very few training experiences. We discuss implications for the development of visual object recognition in both humans and machines.

1 Introduction

The visual objects labeled by common nouns — bowl, cup, chair — are so readily recognized and their names so correctly generalized by young children that early theorists suggested that these “basic-level” categories “carve nature at its joints” (e.g., Gentner (1), Rosch, Mervis, Gray, Johnson and Boyesbraem (2)). This idea is at odds with contemporary understanding of visual object recognition in both human visual science and computer vision. In these literatures, object recognition is seen as a hard and not-yet-solved problem (3-5). If object categories are “given” to young perceivers, theorists of human and machine vision do not know how.

We propose that the answer to how visual object categories are “given” lies in the statistics of infant daily-life visual experiences. In a remarkable case study, Mervis (6) tracked her one-year-old son’s experiences with the category “duck.” There were three very high-frequency instances of that object category: a life-like mallard toy, a soap dish, and a Donald Duck Pez dispenser. Although this one child’s experiences of duck instances are idiosyncratic, all infants’ experiences are constrained by time and place, and therefore likely consist of many repeated experiences of a small set of instances. It is well-established in the literature

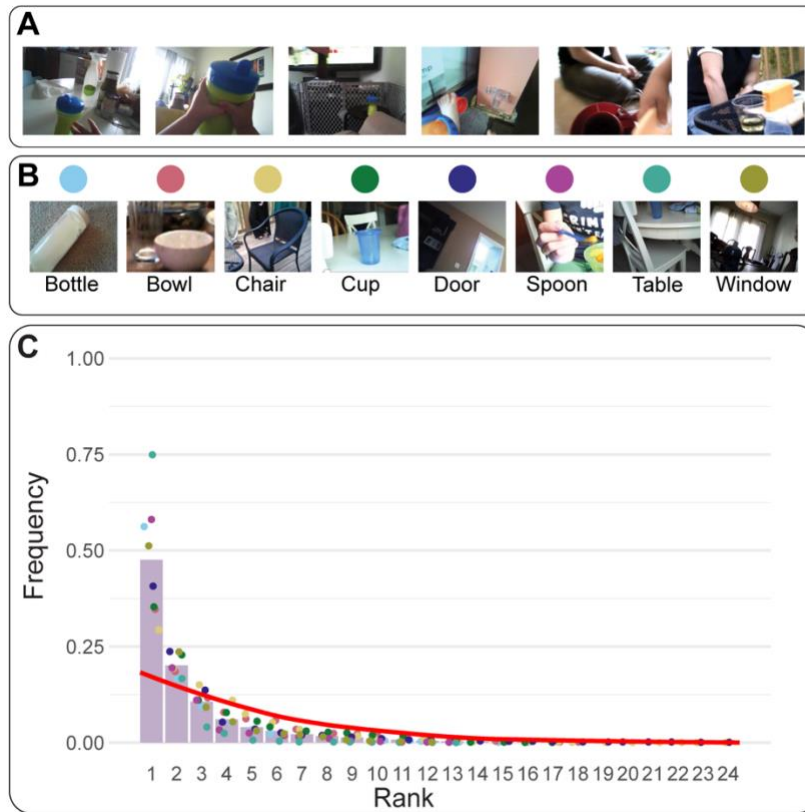


Figure 1. A skewed distribution of infant experiences of instances of early-learned object categories. **(A)** Head-camera images of cups showing different images of the same cup and different images of different cups. **(B)** The 8 target categories **(C)** Mean rank order frequency distribution of unique instances across all mealtimes, normalized as a proportion of all ranks for each category. For each category and subject, we count the number of occurrences of each object instance and rank the instances by frequency in descending order. The colored dots display each category, and the bars illustrate the mean across categories (20,339 datapoints in total). The (smoothed) red line illustrates the null distribution under the hypothesis that infants uniformly sample experiences from the instances present in images recorded in their home.

that infants recognize never-before-seen instances of common object categories (e.g., shoes) as readily as the familiar instances they see most often in their home (e.g., their own shoe, Bergelson and Swingley (7), Campbell and Hall (8), Garrison, Baudet, Breitfeld, Aberman and Bergelson (9)). Adult-like generalization and an assumed limited range of experienced instances are the bases of early theorists’ proposal that these common object categories were visually “given.”

The theoretical consensus in both human cognition (10-12) and machine learning (13-16) is that category learning causes transformations of the raw similarities of instances, changing the feature weights to capture the essential properties of category membership. The empirical consensus, from experimental studies of human learning and from machine learning, is that larger and more diverse training sets lead to better representational spaces and therefore better generalization (17-21). This consensus does not appear to align well with the evidence on the generalized object categories that emerge in infancy. However, in the everyday context of active infants and a 3D world, the images projected from one object to the retina will vary continually and often significantly as a function of the spatial relationship between the object and the perceiver, the lighting, and the surrounding context. Thus, infants’ repeated experiences of an individual object instance — for example, their own sippy cup (Figure 1A) — creates a packet of variable images. Our hypothesis is that the similarity structure of these packets of repeated but varied experiences of a single thing supports efficient category generalization.

We used a corpus of head-camera images collected by infants aged 7 to 11 months ($n = 14$) over a period of several days (22, 23). This is the age range during which robust generalization of common object categories is first evident (7-9). From the corpus, we extracted mealtime episodes, defined as continuous events in which food or dishes were present. Mealtimes are a useful context for our purpose because many of the earliest learned object categories are typically present (23, 24). Further, for infants, mealtimes occur on average 5 times a day and in varied locations and contexts (at a table, on the floor, in a playroom, etc.). Thus, mealtimes offer the opportunity for diversity in the instances and potentially repeated experiences of the same instances.

We provide evidence for the centrality of varied visual experiences of individual instances in infant object categories in three steps. First, we quantify the frequency of unique instances in their visual experiences. Second, using graph theoretic measures, we quantify the similarity structure of repeated experiences of single instances and the aggregated experiences of all instances. Third, in a machine learning experiment, we use artificial training sets with and without the observed similarity structure of infant daily-life experiences and find that very small training sets that mimic the observed similarity structure of infant experiences better support generalization to novel instances.

2 Results

2.1 Infant Visual Experiences of 8 Object Categories

From the corpus of 87 mealtimes, we selected 8 basic-level object categories (25) that were visually frequent in the corpus (22, 23) and that are normatively among the earliest acquired categories for infants developing in the United States (22-24, 26). The 8 categories include both holdable objects (bottle, bowl, cup, spoon) and larger “background” objects (chair, table, door, window). Images were sampled from the mealtime video clips at 0.2 Hz, yielding 11,549 images for analysis. Human coders determined the presence of unique instances of the 8 target categories in each image.

Infant egocentric views were dominated by individual objects in multiple ways. First, infants typically experience instances of a category one at a time; although a single head-camera image often contained instances of more than one of the 8 target categories (a cup and a table, for example), a single image typically contained just one instance of any visually present category (one cup and one table; Fig. S1). Averaged across categories, 0.62 of images containing a given category had exactly one instance of that category ($SD = 0.16$), range 0.37 (chair) to 0.89 (table). Second, within individual mealtimes, a single instance of any present category occurred with high frequency. The single most frequent instance of a visually-present category within a mealtime constituted, on average, 0.61 of all experiences of that category within that mealtime ($SD = 0.14$; range 0.39 for chair to 0.86 for table; Fig. S1), while the three most frequent instances of a visually-present category accounted for, on average, 0.92 of the appearances of that category ($SD = 0.06$; range 0.79 for chair to 0.99 for table). Thus, individual mealtimes present repeated experiences of one or a few instances.

Across the aggregated mealtime experiences of individual infants within and over several days, single instances were also dominant for 7 of the 8 categories (Fig. 1C), accounting on average for 0.48 of all experiences (range across categories from 0.29 for chair to 0.75 for table). Across all mealtimes for an infant, Ranks 1, 2, and 3 constituted on average 0.78 of infant experiences (range across categories 0.64 for chair to 0.96 for table). Thus, across multiple mealtimes, infants experience a small set of the same things with high frequency. If we assume, as the null hypothesis, that infants uniformly sample experiences from the instances present in images recorded in their home (Fig. 1C), then the skewed distribution of observed mealtime instances differs reliably from the null hypothesis (KS test; $D = 0.33$, $p < 0.001$).

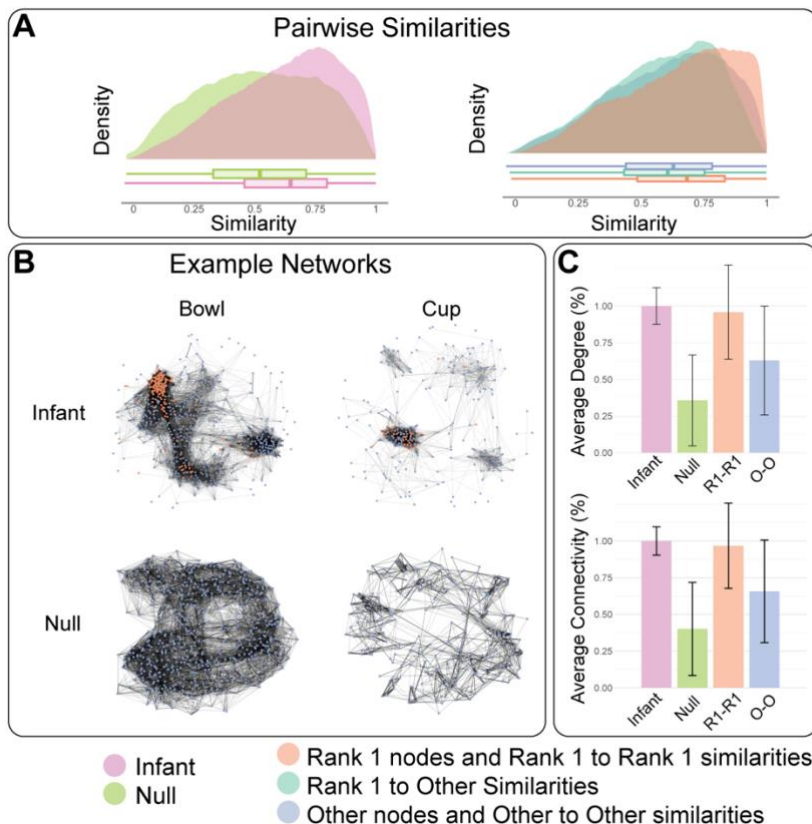


Figure 2. The similarity structure of infant experienced instances. Similarity is measured as RGB histogram correlation $c_{i,j}$ between pairs of images (i, j) . **(A)** Left: Pairwise similarity density aggregated across the eight target categories (1,188,150 datapoints for the observed infant distribution and 97,417 for the null distribution). The box plots illustrate the 0.25, 0.5 (median), and 0.75 quartiles. Right: Observed pairwise similarity density partitioned into three groups of pairs: within Rank 1 pairs (R1-R1), Rank 1 to others (R1-O), and all others (non-Rank 1) to each other (O-O). There are 1,037,730 datapoints in total. See Methods for explanation of differing numbers of data points. **(B)** Top: Example of two observed networks for one infant. Bottom: The corresponding randomly generated networks. Each node represents one image, and the edges indicate pairwise similarities in the top 10% of measured similarities. **(C)** Top: average degree. Bottom: average connectivity. The metrics are further partitioned into Rank 1 nodes (orange) and Other nodes (blue). The error bars illustrate corpus-level standard deviation.

The ubiquity of skewed frequency distributions in human experience is well-known (22, 27-29). Researchers of both human and machine learning have conjectured that these distributions might be beneficial to learning because they provide a combination of both high similarity and high variability (28, 30-33). Although this has been conjectured, it has not been demonstrated at the level of real-world experiences that contain varied views of the same individual object.

To determine the similarity structure of infant experiences, we converted each image to a histogram of RGB color pixel intensities. These raw whole image representations, while not capturing spatial information, are highly effective for recognizing similar objects across multiple views (34-36), and thus provide a useful quantification of similarity for our purposes. We chose a whole image assessment instead of cropping to objects of interest, because infants receive whole images. We computed the similarity (RGB histogram correlation) between all pairs of all mealtime images within a category for each infant (Methods).

The distributions of these within-category pairwise similarities across all within-category images reveal many highly similar pairs but also a wide range of low to very low similarity pairs (Fig. 2A). To determine the contribution of high frequency but varied visual inputs of individual object instances, we partitioned the

overall distribution of similarity pairs for each category and infant into three groups: within Rank 1 pairs (R1-R1), Rank 1 to others (R1-O), and all others (non-Rank 1) to each other (O-O). The distribution of R1-R1 pairs differed from the distribution of R1-O pairs (KS; $D = 0.14$, $p < 0.001$) and from the distribution of O-O pairs (KS; $D = 0.09$, $p < 0.001$), with R1-R1 pairs containing more high-similarity pairs. The mean similarity of R1-R1 pairs was also greater (Wilcoxon rank-sum test, $p < 0.001$; Welch’s two-sample t-test, $p < 0.001$) than R1-O pairs and O-O pairs. However, for all 8 categories, R1-R1 pairs include many dissimilar images (Fig. S1). Finally, the entropy of the observed infant pairwise similarities was less than that of the null distribution (Fig. S1, permutation test, $n=9999$, $p < 0.001$; Methods), indicating greater overall predictability from one image to another in the observed infant experiences than in the null distribution that assumes a uniform sampling of instances. In brief, infant visual experiences create a training set that contains both many high similarity pairs but also many low similarity pairs, with the frequently-repeated instances contributing many high similarity pairs but also some low similarity pairs.

To quantify the mix of high and low similarities in the infant experiences, we created graph theoretic networks for each infant for each of the 8 categories (Fig. 2B). Each node represents an image and the edges between nodes represent the pairwise similarity of the images (Methods). We show (and analyzed) only edges that represent the top 10% of measured similarities. Thus, all edges in the analyzed networks indicate relatively high connectivity in the form of raw similarities that might be expected to activate other experienced images. We also created random networks to instantiate a null hypothesis as follows: for each infant, the observed nodes (specific images) were located uniformly at random within the unit square and then nodes were connected that fell within the top 10% similarity range in the corresponding infant graph (37).

We used two graph-theoretic measures to quantify the properties of the observed and null networks (Fig. 2C). The first measure, average degree, computes the number of edges per node and then averages across nodes (38). Graphs with higher average degree have more direct connections among the individual nodes. Overall, the observed infant graphs showed higher average degrees than the null graphs (Linear Mixed-effects Model [LMM], $p < 0.001$; Methods), indicating that they had more nodes with more direct connections to other nodes. The average degrees for R1-R1 nodes were also greater than for R1-O nodes (LMM, $p < 0.01$) and O-O nodes (LMM, $p < 0.05$) in the observed data. Overall, the higher connectivity in the observed data indicates strong connectivity among all the images experienced by an infant that contain instances of the same category.

Average node connectivity (39) measures the mean number of node-disjoint paths between all image pairs. Higher values indicate greater network robustness: more images (nodes) would need to be removed before pairs of images would become disconnected (no remaining path between the images). The average node connectivity is greater for the infant data than the null (LMM, $p < 0.001$). Average node connectivity is also greater for R1-R1 nodes than for R1-O nodes (LMM, $p < 0.001$) and O-O nodes (LMM, $p < 0.05$) in the observed data. Human learning (and the discovery of category-relevant features) requires the co-activation in memory of individual experiences of the same category (40-42). Thus, a set of category experiences that contains high and low similarity images that are all interconnected could support discovery of the relevant features for broad generalization.

In summary, infant daily-life visual experiences of 8 early-learned object categories consist of many varied experiences of a few individual object instances as well as less frequent experiences of diverse instances. The similarity structure of the aggregated set of experiences is “lumpy,” a mixture of high and low similarity pairs, which yields high raw similarity connectivity within the data set as a whole. The results raise two hypotheses: (1) Data sets that oversample varied views of individual objects are sufficient to create the observed lumpy data structure, and (2) very small sets of training experiences with this lumpy similarity

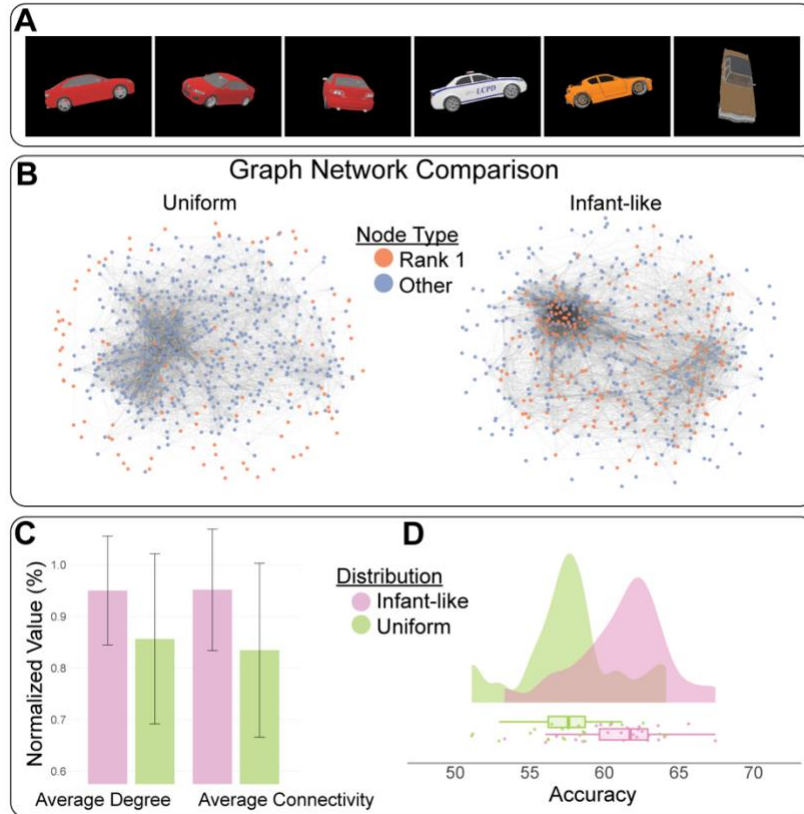


Figure 3. Similarity structure and generalization performance of a machine learning model. **(A)** Sample (cropped) images of the category “car.” The first three images, left to right, illustrate varied views of a single instance. The right-most image illustrates a car instance used for testing that was never seen during training. **(B)** Example networks of the similarity structure of the Uniform and Infant-like training sets for the category car, showing the top 5% of pairwise similarities and lower color opacity for the edges due to denser networks (see Methods, SI). **(C)** The two graph-theoretic measures used to quantify the properties of the Uniform and Infant-like training sets: average degree and average connectivity. The error bars illustrate corpus-level standard deviation. There are 36 networks in total. **(D)** Generalization accuracy achieved by CNNs when trained on different distributions: Infant-like, generated by oversampling varied views of individual instances, and Uniform, which uniformly samples instances and views. All models are tested on the same set of novel instances to measure generalization. There are 48 datapoints.

structure support robust generalization. We next provide evidence relevant to these hypotheses with a machine learning experiment.

2.2 Small, lumpy datasets and generalization

The goal of the machine learning experiment is not to model infant learning but to elucidate the potential role of single-object experiences in supporting category generalization given limited training. We first created artificial training sets by oversampling varied views of single instances using ShapeNet (43) objects (Fig. 3A). For comparison, we also created training sets with Uniform distributions of sampled views from the instances of each category. We purposely constructed very small training sets of 6 categories (airplane, bed, bottle, car, chair, and camera) with ~600 unique images per category (3600 images in total). We created three independent samplings of instances and their varied views to form three unique Infant-like and three corresponding Uniform training sets (Methods).

Our first empirical question is whether an oversampling of varied views of a single object instance along with less frequent sampling of other instances creates a training set with a lumpy similarity structure consistent with the observed infant data. We computed the pairwise similarities between images using

inverse Euclidean distance between GIST features (44), which is more appropriate for the simple ShapeNet images than RGB histogram correlation (Methods). Similarity of pairs was determined within each category for each of the six unique training sets. We then compared the pairwise similarity structure of the training sets using the same measures that we used for the infant experiences: distributions of pairwise similarity, entropy, and the two network measures of connectivity. The distributions of similarities in the Infant-like training sets differed slightly from those in Uniform training sets (KS test, $D = 0.015$, $p < 0.001$), having a more skewed distribution and thus a mixture of high as well as low similarity pairs. However, the structure of pairwise similarities, not the overall similarity distribution, may be the critical factor in efficient learning and generalization. Comparisons of pairwise entropy showed a lower entropy for the Infant-like training data compared to the Uniform data (permutation test, $n=999$, $p < 0.01$; Methods). Finally, the connectivity measures (Fig. 3C) show greater average degree for the Infant-like data than the Uniform data (LMM, $p < 0.05$; Methods) as well as higher average connectivity (LMM, $p < 0.01$).

Our second empirical question is whether training sets with a “lumpier” similarity structure better support generalization. We used the sets of 3600 images to train Convolutional Neural Networks (CNNs) using supervised learning (ResNet-50 from He, Zhang, Ren and Sun (45); Methods). We used supervised learning because infants both hear the names of things and see them, and infants’ generalization of object categories to new instances is usually measured in terms of their generalization of the object name (7-9). Each CNN was trained on one of the three versions of the Infant-like and Uniform training sets and each unique training set was used in 8 independent runs (Methods). The test sets also consisted of 3600 images (exactly 600 per category) of instances not used in training and the same test sets were used for all runs. The Infant-like training sets showed better generalization to novel instances in the test set than did their corresponding Uniform training sets (Fig. 3D). A linear mixed-effects model showed a significant main effect for the dataset distribution ($p < 0.001$; Uniform vs. Infant-like) with no reliable interactions with the three specific versions of training sets. This result supports the hypothesis that a lumpy similarity structure in training images supports generalization from small data sets.

3 General Discussion

Human visual experiences provide relevant information about objects at two levels of granularity. Theories of perception traditionally treated the two levels as two distinct computational problems (46-48). The first, Object constancy, concerns the perception of an individual object as the same thing with the same stable essential properties despite the variability in the 2D images projected to the eye. The second level of granularity, Categorization, concerns the ability to recognize never-seen-before things as members of categories. The two levels of variability are mixed together in daily-life experiences and in daily-life recognition tasks (my sippy cup, my mother’s cup, a new cup). The field does not have a unified understanding of how object constancy and categorization interact in experience-dependent visual development. The present findings indicate that the statistics of the combined variability of images from the same and different things have a similarity structure that may play a critical role in the ability of rank novices, infants, to form generalizable object categories from limited experience. In so doing, the findings make a clear case for increased research on the interplay of object constancy and categorization — behaviorally, neurally, and computationally (3, 4, 46, 49).

The variable views of an individual object instance are often conceptualized in terms of the transformations of the projected image under which the essential properties of the instance remain unchanged (50, 51). Thus, the variation in projected images from a single instance are believed to provide the information to recover those essential properties (50-52). This observation is consistent with studies showing strong predictive links between the variability of images generated by infants when playing with individual objects and their memory for objects and their names (53); see also (19, 54-56). Thus, the mixture of high and low similarity

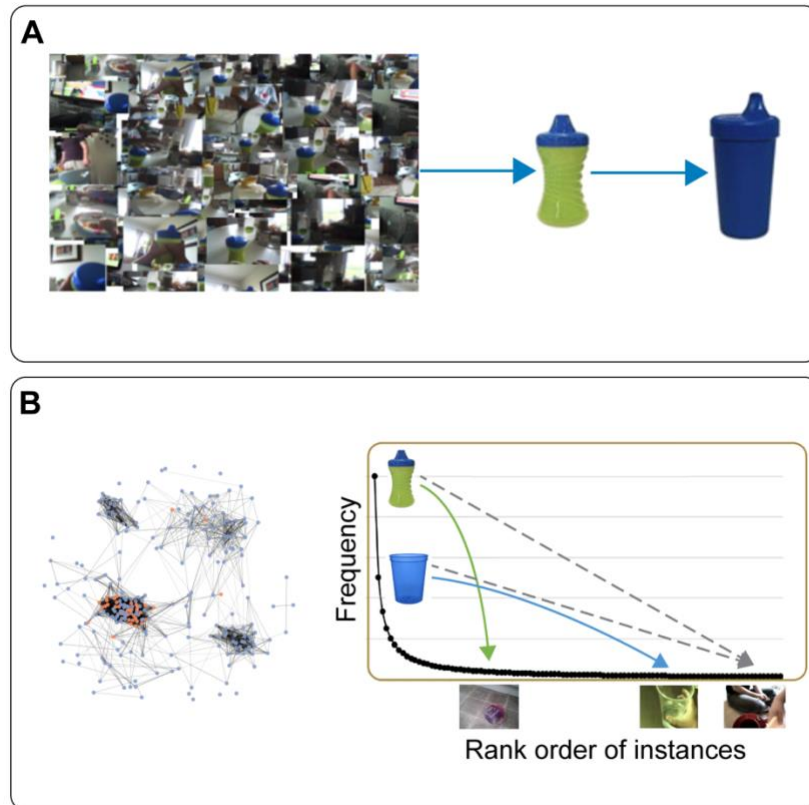


Figure 4. A hypothesis about the relation between object constancy and category generalization from few experienced instances. **(A)** Repeated experiences of a single object yield highly variable images of that object that share the stable properties of the object. Thus, repeated experiences with one object may support generalization to other objects. **(B)** The lumpy similarity structure generated by a mixture of repeated experiences with a few unique instances and rarer experiences with other instances may support the efficient formation of generalizable representations by connecting similar images of different things that then lead to latent knowledge (grey arrows) of the defining properties.

observed in infant experiences of individual things may inform the development of the representational (embedding) space for robust human object recognition.

Infant daily-life experiences contain many repeated episodes of very few things as well as many less-frequent episodes of many things. The present findings show that these aggregate experiences have a lumpy similarity structure of interconnected but distinct clusters of high similarity images. Our conjecture is that the similarity structure observed in the infant data trains both object constancy and categorization. The images projected from a single object instance vary infinitely, but that variation is constrained by how light reflects from the surfaces of things. Thus, the packet of images received from a single instance is constrained by essential properties of the object. We propose that through repeated episodes of variable experiences of a single object instance, the infant may build a unified representation of that one object that forms the basis for a representation space that generalizes to the same kind of thing.

The testable hypothesis is this: If a developing representational space “knows” how the images of one sippy cup can vary, then the representation space may also know something about how the images of a distinct but same kind of thing can also vary (Fig. 4A). A lumpy similarity space in which there are multiple but distinct clusters of high similarity may benefit efficient discovery and integration of the features needed to define an optimal representational space and thus generalization (Fig. 4B). These ideas require empirical and computational examination and clarification. They offer a path to a potential explanation of how infants so readily generalize names for known things to never-before-seen instances of the same category (7-9) and

how, by the time they are 2 ½ years of age, they become one-shot learners (57) that need experience with only one instance to generalize to novel instances in an adult-like manner. The lumpy similarity structure observed in the infant data may not quite “carve nature at its joints,” but it may play a key role in making those joints easier to find.

The findings may also provide practical insights for machine learning. Training sets with a lumpy similarity structure may support learning from small data sets across domains with different relevant stimulus features (30). That is, a lumpy training set may support a learning system’s faster finding of the most relevant features and thus a more optimal embedding space. The use of dataset augmentation in computer vision provides a potential example. Image augmentation is a strategy originally introduced to increase the size of training sets by creating multiple synthetic transformations (e.g., rotations, partial occlusions, cropping, color shifts, Xu, Yoon, Fuentes and Park (58)) of real training images, but that has been found to increase generalization even when training set size is controlled (59). The beneficial effects of this tactic are not yet fully explained (16, 60-63). Transformations of multiple single instances are likely to create a lumpy data set. An interesting question for future research is whether one could systematically decrease the amount of training needed to achieve robust generalization by manipulating the network structure of pairwise similarities and/or the transformations of individual images that create a lumpy structure.

In conclusion, human infants are highly efficient learners of visual object categories. When the efficiency of human learning exceeds that of known learning mechanisms, theorists (64, 65) often postulate the existence of “given” intrinsic knowledge in the form of “inductive biases.” Although the present findings raise many open questions, the results also suggest that a deeper understanding of intrinsic learning mechanisms would benefit from the systematic study of the daily-life visual experiences of objects in infancy, a period characterized by marked advances in the efficiency of visual category learning (7, 9).

4 Methods

4.1 Infant Visual Experiences of 8 Object Categories

Data collection. The corpus of egocentric images during mealtime events is a portion of a larger data set of head-camera videos collected by infants in their homes, $n = 100$, from 3 weeks to 24 months old (66). Parents were taught to place and operate the head cameras and were asked to collect 6 to 8 hours of daily-life experiences; no experimenters were present in the home during data collection. Parents were told that the study was about early visual experiences and that all visual experiences were relevant. The subcorpus of 87 mealtimes (mean duration of a mealtime = 11.22 min., $SD = 11.87$) was extracted. Analyses of the objects in view and the object names heard using the mealtime corpus were reported in two prior studies (22, 23).

Identification of instances in images. Adults (through Amazon Mechanical Turk) were paid to label the objects in each image. (see Clerkin, Hart, Rehg, Yu and Smith (22)). From this coding we selected the 8 target objects that had high frequency in the mealtime corpus and whose names were normatively among the first 100 nouns learned by children learning American English (24). The number of instances in an image and the identity of the individual instances were coded by trained adults in the laboratory. The total number n of object instances per category visible in each image was recorded. Unique alphabetical IDs were assigned to each instance across the entire corpora of data (e.g., spoon A, spoon B, spoon C, etc.) for each category and independently for each infant for images with $n < 4$ instances of the target category. Images with $n \geq 4$ instances of a category are rare and tend to have objects that are too small to identify with certainty. Images with greater than 4 instances for the target category were not included in the determination of pairwise similarities for that category (e.g., in Fig. 2A). Two independent coders coded 20% of the images; image-to-image agreement on the number of instances in an image and the identity of

those instances present both exceeded 84%. Lastly, the unit of analysis is an object occurrence, meaning that an image containing more than one target category is counted as a datapoint for each of those categories.

We detail the computations for all reported measures and figures below.

Number of instances per image. For each category, we use the count of object instances, n , present in each image. We keep images with at least one instance ($n \geq 1$), and group images with $n \geq 4$ together as they are rare. Next, we obtain proportions by dividing the number of images with $n \in \{1, 2, 3, 4\}$ by the total number of images within that category. The resulting proportions per category are the colored dots displayed in Figure S1. To generate the bars, we average the proportions across categories.

Rank frequency within a mealtime. For each category, mealtime, and subject, we count the number of occurrences of each unique object ID present during the mealtime. Then, we rank the object IDs by frequency in descending order, where the rank 1 instance is the one present in the largest number of images within a mealtime. Next, we aggregate the total number of occurrences for each rank across mealtimes and subjects and normalize by the sum of counts to obtain the proportions for each rank. The resulting proportions per category are the colored dots displayed in Figure S1. To generate the bars, we average the proportions across categories.

Rank frequency across mealtimes (Fig. 1, Panel C). Occurrences and ranks are now computed across the entire corpora of data for a given infant (i.e., across mealtime events) rather than within mealtime events. Thus, for a given category, the rank 1 instance is the most frequent object in that category across all recorded experiences of a given infant, and similarly for the remaining ranks. To test for significance against the null distribution, however, we aggregate the raw counts across categories and then normalize by the sum of counts to obtain the exact proportions (i.e., a distribution that adds up to 1.0), rather than averaging the proportions across categories. To generate the null distribution, we uniformly sample an equal total number of counts for each subject and category from the available object IDs for each subject. This is performed 500 times with different seeds for the random number generator (0 through 499) and the raw counts are aggregated across categories and normalized by rank to generate the null frequency distribution (displayed as a smoothed red line in the figure). To test for significance, we use a single seed to have an equal number of counts as in the observed infant data and perform a KS test on the observed (discrete) counts. The number of counts (data points) used for the KS test is 20,339 for each of the observed infant and null distributions, for a total of 40,678 samples.

Similarity analyses. Pairwise similarities were computed using the open-source OpenCV library (67). Histogram correlation $c_{i,j}$ between each pair of images (i, j) is computed in RGB space using 8 histogram bins per channel, for a total of 512 bins. The resulting value $-1 \leq c_{i,j} \leq 1$ is a similarity score, with a higher score denoting a higher similarity. In our results, $c_{i,j} \in (-0.04, 1)$ and thus we set our figure axes to the range $[0, 1]$ for visualization purposes and use all data for the measures. For each category and comparison type, infant subjects with fewer than 10 total images were excluded.

Infant and null similarity density (Fig. 2, Panel A, Left). We illustrate aggregated pairwise similarities across all categories, but the pairwise similarity comparisons are still performed only within-category. We remove duplicate pairwise datapoints that arise after merging categories. The box plots illustrate the 0.25, 0.5 (median), and 0.75 quartiles. There are 1,188,150 datapoints in total for the infant distribution. To generate the null distribution, we selected all instances that had at least 5 images, for each category and subject. Then we sampled an equal number of images per instance based on the instance with the fewest images. We filtered out subjects with fewer than 10 resulting images across all instances. Next, for each category, we identified the subject who had the fewest images and sampled uniformly (across instances) that number of images from each subject. Lastly, we compute pairwise similarities among the resulting set

of images. This yielded a null distribution with 97,417 datapoints, for a total of 1,285,567. We computed their entropy by discretizing the range $[0, 1.04]$ into 100 bins. The bars in Fig. S1 illustrate the entropy of all pairwise similarities (1,285,567 datapoints), and the colored dots illustrate the entropy of each category independently. In the latter case, the Infant distribution contains 1,519,564 datapoints instead of 1,188,150 datapoints as duplicates across categories were not removed.

Infant similarity density by group (Fig. 2, Panel A, Right). We used an analogous procedure to Fig. 2A (Left), but now grouped by rank. For each group, we filtered out subjects with less than 10 images and removed duplicate pairwise datapoints that arose after merging categories. The total number of datapoints across all categories and groups was now 1,037,730. The similarity density by category is illustrated in Fig. S1, which contains a total of 1,117,337 datapoints as the categories were treated independently and thus duplicate pairwise datapoints were not removed.

Graph networks (Fig. 2, Panel B). Each image served as a node connected by similarity-weighted edges. Average connectivity was computed using the `average_node_connectivity` function in the open-source NetworkX library (68). Metrics that require fully connected networks, such as average connectivity, were computed for each connected component and then a weighted average across components was calculated, where the weight is the number of node pairs in each component. Single-node components (i.e., disconnected nodes) were not included in such network metrics. The proportion of connected nodes in the Infant and Null graphs was on average 0.80 (SD = 0.12) and 0.74 (SD = 0.29), respectively. For average node degree, disconnected nodes contribute a degree of zero. The null networks were generated for each subject and category, excluding those with fewer than 10 nodes (images). For each of the Null and observed Infant data, there were 95 networks with at least 10 nodes. For each of the R1-R1 and O-O subgroups, there were 60 such networks, and for the R1-O subgroup there were 43 networks. The linear mixed-effects models had distribution (Infant or Null) and categories as fixed effects and optionally an intercept for the infant subjects. For illustration purposes, graph measures were averaged first across infants for each category, then normalized to the range $[0.0, 1.0]$ by max-division between infant and null graph pairs, and lastly averaged across categories. The error bars illustrate corpus-level standard deviation.

Statistical analysis of aggregate measures. We used the large number of continuous data points specified above for several statistical measures, such as to compare means between two distributions using Welch’s t-test. However, other measures such as entropy represent a single aggregate number for several thousand or million datapoints. As such, it is not possible to compute test statistics on a single observation, so we used permutation tests. To do so, we first computed the measure (e.g., entropy) for the entire corpus of data and recorded the difference between Infant and Null. Under the null hypothesis, we should observe similar differences simply by chance, regardless of the data distribution label (Infant or Null). Hence, for n iterations, we sampled subsets of size K , randomly permuted the labels of the K sampled datapoints, and computed the difference in measures (e.g., entropy) for the permuted subsets. The resulting p-value is the fraction of times that such an extreme difference is observed by chance. For the entropy permutation tests, we used $n = 9,999$ permutations and sampled 25% of the datapoints at each iteration. For the computational data that follows, we used $n = 999$ and sampled 20% of the datapoints, as the corpus is larger. Lastly, as complementary non-permutation tests, we also computed the entropy of the n unpermuted subsamples and performed a Welch’s two-sample t-test and a Wilcoxon rank-sum test on these n estimates. These yielded results consistent with the permutation test for both the observed infant data and computational data ($p < 0.001$).

4.2 Small lumpy datasets and generalization

Training and test sets. Training and testing data sets were created from a subset of the publicly-available ShapeNet dataset of three-dimensional objects (43). We generated two-dimensional images from

ShapeNet’s 3D object models using rendering software developed by us. Six object categories were used: airplane, bed, bottle, car, chair, and camera. Eight object instances were used for each category, for a total of 48 instances. To measure generalization performance, two instances per category were excluded from training and only presented to the model at test time. Moreover, out of the six training instances per category, one was randomly chosen to be the Rank 1 instance. For fairness, the exact same test images were used in all experiments, and the train and test sets are composed of 3,600 images each (1:1 ratio).

We created the 3 unique instantiations of the Infant-like and Uniform training sets (6 in total) as follows. For the first instantiation, denoted as “Random,” we generated a set of views for each instance by rendering it at random 3D orientations and saving each view as an image. We generated 600 views per object instance. To do this, we sampled a set of random orientations (Euler angles) exactly once from a uniform distribution in the range $[-180, 180]$ and used the same set of angles for all objects. Although this simple sampling approach does not produce a perfectly uniform distribution over the rotation group $SO(3)$, it provides a broad and approximately isotropic coverage. For the Infant-like training set, from this generated set of views of 6 instances per category we then oversampled one randomly-selected instance to yield a rank 1 instance, and then uniformly sampled the remaining set. The amount of skew in the infant distribution was based on the infant who contributed the most data, on average 35% Rank 1 instances across all categories.

For the two remaining instantiations, we generated views near two different characterizations of optimal views for visual learning in the literature: Planar views (major axis perpendicular or parallel to the line of sight) and 45° views, which show multiple sides of the object (69). To generate diverse object views for training on these two classes of views, starting from the six pre-defined orientations (69), slight random rotations (i.e., perturbations) were applied to the objects within ± 15 degrees of each pre-defined orientation. Again, the Infant-like and Uniform data sets were created by oversampling more views from one instance or by uniformly sampling views from all instances to yield training sets of 3,600 images. The sampling of 3,600 training images was done across categories, yielding roughly ~ 600 images per category.

The test set was identical for all training sets: exactly 600 images per category generated through the procedure for random views, but ensuring 600 images per category. We used 12 instances (two per category) not included in the training sample and generated 300 images per instance, for a total of 3,600 test images.

Implementation. We used Pytorch’s (70) implementation of a ResNet-50 Convolutional Neural Network (45), and trained all models using a cross-entropy loss and an SGD momentum optimizer on an NVIDIA Titan X GPU. Hyperparameters were defined initially and kept fixed throughout the experiments: learning rate = 10^{-3} , momentum = 0.9, weight decay = 10^{-3} , batch size = 100. The learning rate was decreased once by 10% at epoch 30 out of 50. Models were trained from scratch eight times on each dataset and the test accuracy of all runs is presented in Figure 3D.

Input dataset statistics. We computed pairwise Euclidean distance between images in GIST feature space (44), which is suitable for these less complex (no-background) images. Our graph networks used edges within the top 5% similarity due to a greater number of pairs in the training sets than in the observed infant data. The conclusions for average degree are the same if we use the top 10% (LMM, $p < 0.05$); the computations for average connectivity become computationally expensive due to the larger number of connected pairs (cf. average degree in Table S1), prompting us to use a threshold of 5% for both measures. The overall proportion of connected nodes is also illustrated in Table S1. When using linear mixed-effects models to test significance, the different data set instantiations were treated as the random variable in the data analyses. All other measures follow the methods used in the infant data analyses.

4.3 Data & code availability

The raw video data were collected under Indiana University IRB protocol #1505862312. Because the head-camera video was collected without constraints, the images contain faces of unconsented individuals as well as information through which specific families could be identified. Consequently, the sharing of the videos is not ethical and not allowed under the protocol. The coding of head-camera images for objects present and their identity by participant number and category that do not contain identifiable information or faces will be deposited to the Databrary repository at <https://databrary.org/> and available to researchers with IRB approval from their own institutions. The datasheets of number and identity of instances as well as the code for all analyses will be available at an Open Science Framework (OSF) repository ([here](#)).

Acknowledgements

The research was supported by NIH-NICHD award 5R01HD104624 and NIH-NEI award 1R01EY032897 to L.B.S. and D.J.C.

References

1. D. Gentner, Why Nouns Are Learned before Verbs: Linguistic Relativity Versus Natural Partitioning. *BBN report ; no. 4854. Center for the Study of Reading Technical Report ; no. 257.* (1982).
2. E. Rosch, C. B. Mervis, W. D. Gray, D. M. Johnson, P. Boyesbraem, Basic Objects in Natural Categories. *Cognitive Psychol* **8**, 382–439 (1976).
3. V. Ayzenberg, M. Behrmann, The Dorsal Visual Pathway Represents Object-Centered Spatial Relations for Object Recognition. *J Neurosci* **42**, 4693–4710 (2022).
4. V. Ayzenberg, M. Behrmann, Development of visual object recognition. *Nat Rev Psychol* **3**, 123–137 (2024).
5. N. Pinto, D. D. Cox, J. J. DiCarlo, Why is real-world visual object recognition hard? *PLoS Comput Biol* **4**, e27 (2008).
6. C. B. Mervis, "Child-basic object categories and early lexical development" in *Concepts and Conceptual Development: Ecological and Intellectual Factors in Categorization*, U. Neisser, Ed. (Cambridge University Press, Cambridge, 1987), chap. 201-233.
7. E. Bergelson, D. Swingley, At 6–9 months, human infants know the meanings of many common nouns. *Proceedings of the National Academy of Sciences* **109**, 3253–3258 (2012).
8. J. Campbell, D. G. Hall, The scope of infants' early object word extensions. *Cognition* **228** (2022).
9. H. Garrison, G. Baudet, E. Breitfeld, A. Aberman, E. Bergelson, Familiarity plays a small role in noun comprehension at 12-18 months. *Infancy* **25**, 458–477 (2020).
10. R. M. Nosofsky, Attention, Similarity, and the Identification-Categorization Relationship. *J Exp Psychol Gen* **115**, 39–57 (1986).
11. R. N. Shepard, Stimulus and Response Generalization: A Stochastic Model Relating Generalization to Distance in Psychological Space. *Psychometrika* **22**, 325–345 (1957).
12. R. N. Shepard, Toward a Universal Law of Generalization for Psychological Science. *Science* **237**, 1317–1323 (1987).
13. S. Edelman, Representation is representation of similarities. *Behav Brain Sci* **21**, 449–+ (1998).
14. R. Hadsell, S. Chopra, Y. LeCun (2006) Dimensionality Reduction by Learning an Invariant Mapping. in *IEEE/CVF Conference on Computer Vision and Pattern Recognition (CVPR)*, pp 1735–1742.
15. P. Khosla *et al.*, Supervised Contrastive Learning. *Advances in Neural Information Processing Systems* **33**, *NeurIPS 2020* **33** (2020).

16. A. Krizhevsky, I. Sutskever, G. E. Hinton, ImageNet Classification with Deep Convolutional Neural Networks. *Commun Acm* **60**, 84–90 (2017).
17. Y. Bahri, E. Dyer, J. Kaplan, J. H. Lee, U. Sharma, Explaining neural scaling laws. *P Natl Acad Sci USA* **121** (2024).
18. J. Kaplan *et al.*, Scaling Laws for Neural Language Models. <http://dx.doi.org/https://doi.org/10.48550/arXiv.2001.08361>.
19. L. Raviv, G. Lupyán, S. C. Green, How variability shapes learning and generalization. *Trends in Cognitive Sciences* **26**, 462–483 (2022).
20. C. Sun, A. Shrivastava, S. Singh, A. Gupta (2017) Revisiting Unreasonable Effectiveness of Data in Deep Learning Era. in *2017 IEEE/CVF International Conference on Computer Vision (ICCV)*, pp 843–852.
21. R. Taori *et al.*, Measuring Robustness to Natural Distribution Shifts in Image Classification. *Advances in Neural Information Processing Systems 33, NeurIPS 2020* **33** (2020).
22. E. M. Clerkin, E. Hart, J. M. Rehg, C. Yu, L. B. Smith, Real-world visual statistics and infants' first-learned object names. *Philosophical Transactions of the Royal Society B: Biological Sciences* **372** (2017).
23. E. M. Clerkin, L. B. Smith, Real-world statistics at two timescales and a mechanism for infant learning of object names. *Proceedings of the National Academy of Sciences* **119** (2022).
24. M. C. Frank, M. Braginsky, D. Yurovsky, V. A. Marchman, Wordbank: an open repository for developmental vocabulary data. *Journal of Child Language* **44**, 677–694 (2016).
25. E. Rosch, "Principles of categorization" in *Cognition and categorization*, E. Rosch, B. B. Lloyd, Eds. (Lawrence Erlbaum Associates, 1978), pp. 27–48.
26. L. Fenson *et al.*, Variability in Early Communicative Development. *Monogr Soc Res Child* **59**, R5–+ (1994).
27. S. T. Piantadosi, Zipf's word frequency law in natural language: A critical review and future directions. *Psychonomic Bulletin & Review* **21**, 1112–1130 (2014).
28. L. B. Smith, S. Jayaraman, E. Clerkin, C. Yu, The Developing Infant Creates a Curriculum for Statistical Learning. *Trends in Cognitive Sciences* **22**, 325–336 (2018).
29. G. K. Zipf, *Human behavior and the principle of least effort* (Addison-Wesley Press, 1949).
30. P. F. Carvalho, R. L. Goldstone, Putting category learning in order: Category structure and temporal arrangement affect the benefit of interleaved over blocked study. *Mem Cognition* **42**, 481–495 (2014).
31. S. C. Y. Chan *et al.*, Data Distributional Properties Drive Emergent In-Context Learning in Transformers. *Adv Neur In* **35** (2022).
32. Y. J. Lee, K. Grauman (2011) Learning the Easy Things First: Self-Paced Visual Category Discovery. in *IEEE/CVF Conference on Computer Vision and Pattern Recognition (CVPR)*, pp 1721–1728.
33. R. Salakhutdinov, A. Torralba, J. Tenenbaum (2011) Learning to share visual appearance for multiclass object detection. in *IEEE/CVF Conference on Computer Vision and Pattern Recognition (CVPR)*, pp 1481–1488.
34. J. Domke, Y. Aloimonos (2006) Deformation and Viewpoint Invariant Color Histograms. in *Proceedings of the British Machine Vision Conference 2006*, pp 53.51–53.10.
35. M. J. Swain, D. H. Ballard, Color Indexing. *International Journal of Computer Vision* **7**, 11–32 (1991).
36. J. B. Luo, D. Crandall, Color object detection using spatial-color joint probability functions. *IEEE T Image Process* **15**, 1443–1453 (2006).
37. M. Penrose, *Random Geometric Graphs* (Oxford University Press, ed. 1st, 2003).
38. R. Diestel, *Graph Theory*, Graduate Texts in Mathematics (Springer Berlin Heidelberg, ed. 6, 2025), 10.1007/978-3-662-70107-2.
39. L. W. Beineke, O. R. Oellermann, R. E. Pippert, The average connectivity of a graph. *Discrete Math* **252**, 31–45 (2002).

40. C. R. Bowman, T. Iwashita, D. Zeithamova, Tracking prototype and exemplar representations in the brain across learning. *Elife* **9** (2020).
41. M. L. Schlichting, A. R. Preston, Memory integration: neural mechanisms and implications for behavior. *Curr Opin Behav Sci* **1**, 1–8 (2015).
42. M. T. R. van Kesteren, D. J. Ruiter, G. Fernández, R. N. Henson, How schema and novelty augment memory formation. *Trends Neurosci* **35**, 211–219 (2012).
43. A. X. Chang *et al.*, ShapeNet: An Information-Rich 3D Model Repository. <http://dx.doi.org/10.48550/arXiv.1512.03012>.
44. A. Oliva, A. Torralba, Modeling the Shape of the Scene: A Holistic Representation of the Spatial Envelope. *International Journal of Computer Vision* **42**, 145–175 (2001).
45. K. M. He, X. Y. Zhang, S. Q. Ren, J. Sun (2016) Deep Residual Learning for Image Recognition. in *IEEE/CVF Conference on Computer Vision and Pattern Recognition (CVPR)*, pp 770–778.
46. J. J. DiCarlo, D. D. Cox, Untangling invariant object recognition. *Trends in Cognitive Sciences* **11**, 333–341 (2007).
47. D. Marr, H. K. Nishihara, Representation and recognition of the spatial organization of three-dimensional shapes. *Proceedings of the Royal Society of London. Series B. Biological Sciences* **200** (1978).
48. T. Poggio, S. Edelman, A network that learns to recognize three-dimensional objects. *Nature* **343**, 263–266 (1990).
49. J. J. DiCarlo, D. Zoccolan, N. C. Rust, How does the brain solve visual object recognition? *Neuron* **73**, 415–434 (2012).
50. J. J. Gibson, *The ecological approach to visual perception* (Houghton, Mifflin and Company, 1979).
51. M. Graf, Coordinate transformations in object recognition. *Psychol Bull* **132**, 920–945 (2006).
52. J. T. Todd, The visual perception of 3D shape. *Trends in Cognitive Sciences* **8**, 115–121 (2004).
53. L. K. Slone, L. B. Smith, C. Yu, Self-generated variability in object images predicts vocabulary growth. *Developmental Sci* **22** (2019).
54. K. H. James, S. S. Jones, L. B. Smith, S. N. Swain, Young Children's Self-Generated Object Views and Object Recognition. *J Cogn Dev* **15**, 393–401 (2014).
55. O. S. Kingo, P. Krojgaard, Object manipulation facilitates kind-based object individuation of shape-similar objects. *Cognitive Dev* **26**, 87–103 (2011).
56. S. Stojanov *et al.*, Incremental Object Learning from Contiguous Views. *2019 IEEE/CVF Conference on Computer Vision and Pattern Recognition (CVPR)* 10.1109/Cvpr.2019.00898, 8769–8778 (2019).
57. L. B. Smith, S. S. Jones, B. Landau, L. Gershkoff-Stowe, L. Samuelson, Object name learning provides on-the-job training for attention. *Psychol Sci* **13**, 13–19 (2002).
58. M. Xu, S. Yoon, A. Fuentes, D. S. Park, A Comprehensive Survey of Image Augmentation Techniques for Deep Learning. *Pattern Recognition* **137** (2023).
59. T. Chen, S. Kornblith, M. Norouzi, G. Hinton, A Simple Framework for Contrastive Learning of Visual Representations. *Pr Mach Learn Res* **119** (2020).
60. R. Balestriero, L. Bottou, Y. LeCun, The Effects of Regularization and Data Augmentation are Class Dependent. *Adv Neur In* **35** (2022).
61. T. Devries, G. W. Taylor, Improved Regularization of Convolutional Neural Networks with Cutout.
62. C. F. G. Dos Santos, J. P. Papa, Avoiding Overfitting: A Survey on Regularization Methods for Convolutional Neural Networks. *ACM Computing Surveys* <https://doi.org/10.1145/3510413>, Article 123 (2022).
63. G. Zhang, M. Cisse, Y. Dauphin, D. Lopez-Paz (2018) mixup: Beyond Empirical Risk Minimization. in *International Conference on Learning Representations (ICLR)*.
64. B. M. Lake, R. Salakhutdinov, J. B. Tenenbaum, Human-level concept learning through probabilistic program induction. *Science* **350**, 1332–1338 (2015).
65. F. H. Sinz, X. Pitkow, J. Reimer, M. Bethge, A. S. Tolias, Engineering a Less Artificial Intelligence. *Neuron* **103**, 967–979 (2019).

66. C. M. Fausey, S. Jayaraman, L. B. Smith, From faces to hands: Changing visual input in the first two years. *Cognition* **152**, 101–107 (2016).
67. G. Bradski, The OpenCV library. *Dr Dobbs J* **25**, 120–+ (2000).
68. A. A. Hagberg , D. A. Schult , P. J. Swart (2008) Exploring network structure, dynamics, and function using NetworkX. in *Python in Science*, eds G. Varoquaux , T. Vaught, J. Millman (Pasadena, CA USA), pp 11–15.
69. A. F. Pereira, K. H. James, S. S. Jones, L. B. Smith, Early biases and developmental changes in self-generated object views. *Journal of Vision* **10**, 22–22 (2010).
70. A. Paszke *et al.*, PyTorch: An Imperative Style, High-Performance Deep Learning Library. *2019 Advances in Neural Information Processing Systems 32 (NeurIPS)* **32** (2019).

Supplementary Information

Infant Visual Experiences of 8 Object Categories

We present in Fig. S1 a visualization of results mentioned in the Main Text.

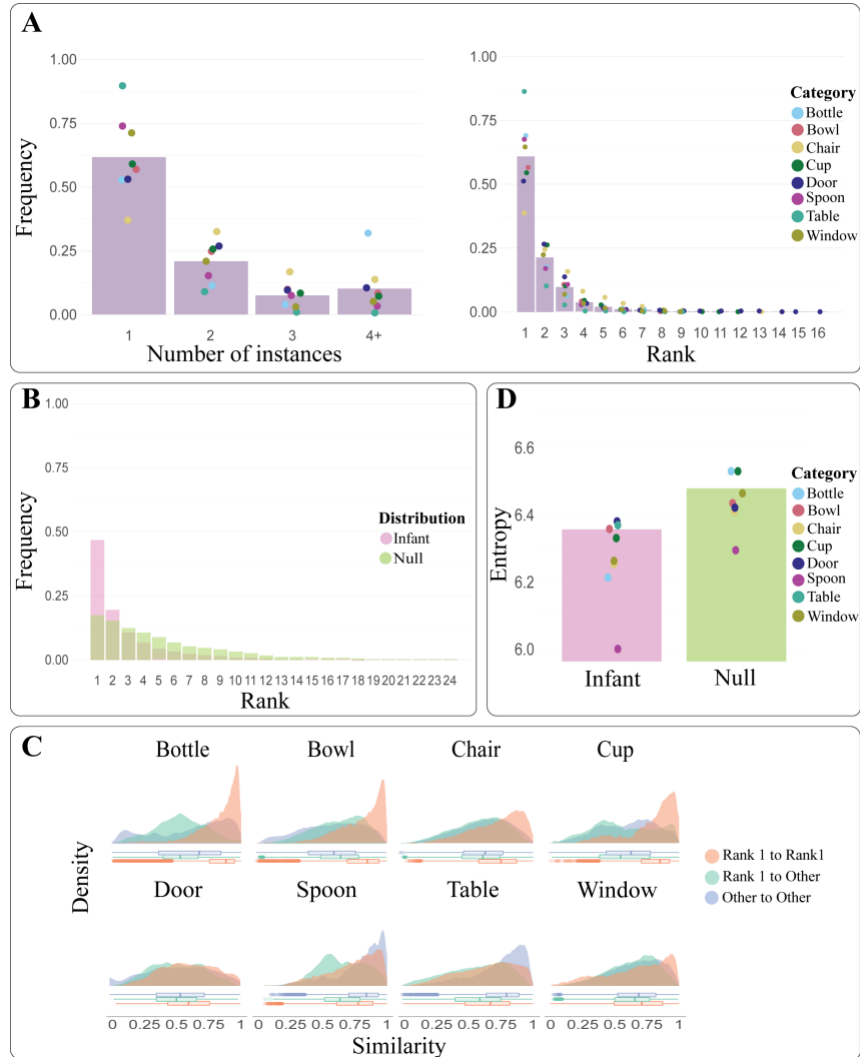


Figure S1. Several characterizations of infant mealtime experiences. **(A) Left:** Number of instances per image for each category. Infants tend to see one category member at a time; e.g., one cup, one bowl. **Right:** Frequency distribution by rank within a mealtime; i.e., the ranks are determined within each mealtime and then aggregated across mealtimes. We see that the Rank 1 instance within a mealtime tends to dominate. The bars illustrate the average across categories. **(B)** Frequency distribution by rank across mealtimes. Here, we show the non-smoothed null distribution instead of a smoothed version as in Fig. 1. **(C)** Observed pairwise similarity density by category, partitioned into three groups of pairs: within Rank 1 pairs (R1-R1), Rank 1 to others (R1-O), and all others (non-Rank 1) to each other (O-O). There are 1,117,337 datapoints in total. **(D)** Entropy of pairwise similarities for each distribution, discretized using 100 bins. The bars illustrate the entropy of all pairwise similarities (1,285,567 datapoints), and the colored dots illustrate the entropy of each category independently. The latter contains a total of 1,616,981 datapoints as categories are treated independently and thus duplicates across categories are not removed for the Infant distribution.

Small, lumpy datasets and generalization

Input dataset statistics. We provide additional input dataset statistics in Table S1, where we observe that relaxing the network similarity threshold from 5% to 10% roughly doubles the average node degree, which in turn makes computing average connectivity computationally expensive. Thus, we use a threshold of 5% for both measures.

DATASET	PROPORTION OF CONNECTED NODES		AVERAGE DEGREE	
	TOP 5%	TOP 10%	TOP 5%	TOP 10%
Uniform	0.94 ± 0.03	0.97 ± 0.02	23.6 ± 4.4	49.0 ± 8.4
Infant-like	0.94 ± 0.02	0.97 ± 0.01	26.3 ± 3.4	54.0 ± 6.4

Table S1. Graph network measures by distribution using different edge similarity thresholds for connecting nodes. Each dataset measure is averaged across its three subkinds. While the proportion of connected nodes is similar regardless of the threshold used, the average degree roughly doubles when relaxing the threshold from 5 to 10%. Corpus-level standard deviation is shown. Proportions are out of 1.0.

Robustness. To test whether 8 runs are robust enough for the experiments in the Main Text, we train an additional 80 runs on the Uniform distribution with two different subkinds. The results are displayed in Table S2. Since the mean accuracy and standard deviation between 8 and 80 runs are similar for both subkinds, we conclude that 8 runs are robust enough.

DATASET	ACCURACY (8 RUNS)	ACCURACY (80 RUNS)
Uniform (<i>Subkind 1</i>)	0.5727 ± 0.03	0.5796 ± 0.03
Uniform (<i>Subkind 2</i>)	0.5854 ± 0.03	0.5848 ± 0.03

Table S2. Robustness test of CNN generalization accuracy. We test robustness by training 8 and 80 independent runs on two dataset subkinds and observe similar mean accuracies in both cases. Thus, we perform 8 runs per dataset in the Main Text.